PDF-XChange Viewer Click to buy NOW! www.docu-track.com
PDF-XChange Viewer Click to buy NOW! www.docu-track.com

A Variational, Non-Parametric Approach to the Fuzzy Segmentation of Diffusion Tensor Images

Sebastiano Barbieri[1], Miriam H.A. Bauer[2], Jan Klein[1], Christopher Nimsky[2], and Horst K. Hahn[1]

[1] Fraunhofer MEVIS - Institute for Medical Image Computing, Universitätsallee 29, 28359 Bremen, Germany
[2] Department of Neurosurgery, University of Marburg, Baldingerstrasse, 35033 Marburg, Germany

Abstract. This paper presents a novel variational approach for the segmentation of diffusion tensor images (DTI). After a certain fiber bundle has been tracked by means of an arbitrary fiber tracking algorithm, we suggest to use the DTI segmentation algorithm to better determine the true borders of the fiber bundle. Specifically, we perform kernel density estimations of the probability density functions (PDFs) of the principal diffusion directions in the foreground - to be segmented - and the background. Thus, we choose a non-parametric approach and do not make any assumption on the distribution of the underlying data. The estimated PDFs are employed to construct a novel energy functional to be minimized. The energy functional contains a fuzzy membership function and a regularization term, to guarantee the smoothness of the resulting segmentation. A robust and efficient two-phase method is used to minimize the energy functional and simultaneously update the density functions. The algorithm is validated on both simulated DTI phantoms and real data.

Keywords: Brain, Diffusion Tensor Imaging, Fiber Tracking, Fuzzy Segmentation, Parzen Density Estimate, Non-Parametric

1 Introduction

Diffusion tensor imaging (DTI) is a magnetic resonance imaging method which allows to measure the anisotropic diffusion of water molecules in in-vivo biological tissue such as white matter (WM) in the brain [9,31,28]. An important application of DTI is fiber tractography, which assumes that the principal diffusion direction matches the orientation of the corresponding underlying fiber system and thus allows the reconstruction of the 3D architecture of WM fiber pathways [8,25,29]. In recent years, fiber tractography has become well established in the research environment with first clinical uses being reported.

A drawback of many streamline tractography algorithms is that the extent of the tracked fiber bundle is often underestimated [7]. For this reason, we suggest a variational approach to the segmentation of diffusion tensor images which may

PDF-XChange Viewer Click to buy NOW! www.docu-track.com
PDF-XChange Viewer Click to buy NOW! www.docu-track.com

be used as a postprocessing step for fiber tracking when it is crucial to precisely estimate the true border location of the bundle. In further detail, the voxels pierced by a tracked fiber are used to initialize the segmentation algorithm.

In [27], a fuzzy region competition algorithm for the segmentation of scalar valued images has been proposed. In this work, we illustrate how some of those ideas may be adapted to segment diffusion tensor images. Moreover, for the sake of efficiency, we suggest a simplified version of the energy functional to be minimized. The functional is composed of a fuzzy competition term and a regularization term. The competition term drives the solution toward the most likely region (the tract to be segmented or the background) based upon kernel density estimations of the PDFs of the principal diffusion directions, whereas the regularization term guarantees smooth segmentation results. A minimizer of the functional, which is robust with respect to the initialization and efficiently computed, may be obtained by using the two-phase algorithm presented in [11]. Segmentation results may be visualized in 2D as color coded likelihood maps of a voxel being part of the segmented tract, or (after thresholding) in 3D as semi-transparent hulls around the tracked fibers.

Possible applications of the algorithm include determining the exact location of the boundaries of a certain fiber bundle when planning a neurosurgical procedure or a more precise quantization of the atrophy of different white matter structures in dementia patients.

Structure of the paper. After discussing related work in Section 2, we detail the segmentation method in Section 3. In particular, we illustrate the two phases of the algorithm: the estimation of the probability density functions in Section 3.1 and the minimization of the energy functional in Section 3.2. Moreover, in Section 3.4, we suggest simple ways of making the segmentation algorithm act locally on the image. Results on modeled DTI software phantoms and on a real patient dataset are shown in Section 4 and some concluding remarks are made in Section 5.

2 Related Work

The problem of segmenting diffusion tensor data has received increasing attention in recent years. In [33], a crisp segmentation algorithm based on k-means clustering is presented with the goal of partitioning the thalamus into its different nuclei. As a distance measure, the k-means approach employs a linear combination of the Mahalanobis distance between voxel coordinates and the Frobenius norm of the difference between the two diffusion tensors at those coordinates.

The work of [34] similarly aims at segmenting thalamic nuclei from DTI, and by making use of spectral clustering and Markovian relaxation, presents the advantage of not having to explicitly define the centers of the clusters. Compared to these two approaches, in the context of tract reconstruction, fuzzy segmentation algorithms have the advantage that they can be used to determine voxels which present partial volume effects, such as the contemporary presence of different

PDF-XChange Viewer Click to buy NOW! www.docu-track.com
PDF-XChange Viewer Click to buy NOW! www.docu-track.com

grey matter tracts, or of different tissues such as grey matter and cerebrospinal fluid.

In [4,5,3] an interesting fuzzy and nonparametric approach to DTI segmentation is suggested. The approach makes use of the tensor representation in the Log-Euclidean framework [1] and information theory to cluster tensors belonging to a specific tract. However, from our experience, the Log-Euclidean similarity-invariant distance between tensors is very sensitive to changes in tensor eigenvalues and less sensitive with respect to changes in the principal diffusion direction, which leads to segmentation results which are able to distinguish very well between clusters of different anisotropy, but to a lesser extent between tensor clusters which differ only slightly with respect to the principal diffusion direction. For this reason, in this paper we concentrate our analysis on the distribution of the principal diffusion direction in the different tensor clusters.

In [10], a weighted graph is constructed with a number of vertexes corresponding to the number of image voxels and weights assigned to the edges based on the difference in fractional anisotropy between tensors at neighboring voxels. Binary tract extraction is obtained by means of an s-t cut of the graph. We compare the segmentation results of this min-cut based algorithm to the results of the variational approach suggested in this paper.

3 Methods

We start by computing an initial estimate of the fiber tract to be segmented by means of the streamline tractography algorithm presented in [32]. However, any other tractography algorithm may be used. Let us denote the vector-valued image containing the principal diffusion directions estimated in each voxel by I. Further, define a fuzzy membership function u over the domain Ω of I, constrained to take values in the interval $[0, 1]$. A higher value of u at voxel x corresponds to a higher likelihood for the voxel x to be part of the tract we would like to segment. Initially, we set $u = 1$ at voxels through which the tracked fibers go (the foreground of the image) and $u = 0$ elsewhere (the background of the image). Next, we apply a two-phase fuzzy region competition algorithm, described in its general form in [26]. In the version of the algorithm presented in this work, the algorithm alternates between estimating the probability density functions (PDFs) of principal diffusion directions in the foreground and background of the image and finding a fuzzy membership function u that minimizes a specific energy functional. These two steps are described in detail in the next sections.

3.1 Estimation of the Probability Density Functions

Let us denote the PDF of the principal diffusion direction at voxels belonging to the tracked bundle by p_1 and the PDF of the principal diffusion direction at voxels belonging to the background by p_2. Because the sense of principal diffusion directions is unknown, we may restrict our computations to the upper hemisphere of the 2-sphere S^2, which we denote by $\mathcal{A}$. To this end, for n approximately evenly

PDF-XChange Viewer Click to buy NOW! www.docu-track.com
PDF-XChange Viewer Click to buy NOW! www.docu-track.com

distributed points $\{a\}$ on $\mathcal{A}$ we evaluate

$$p_1(a) = \frac{1}{\|u\|_1} \int_\Omega u(x) K(a, I(x))\, dx \tag{1}$$

$$p_2(a) = \frac{1}{\|1-u\|_1} \int_\Omega (1-u(x)) K(a, I(x))\, dx \tag{2}$$

where $\|u\|_1 = \int_\Omega u(x)\, dx$ and K is a weighting function. Specifically, Equations (1) and (2) correspond to continuous versions of weighted Parzen density estimates [30]. Although possible appropriate choices for the kernel K are manifold, we use the von Mises-Fisher distribution [2,23] on S^2 with mean direction μ and concentration parameter κ

$$K(a, \mu) = C_3(\kappa) \exp(\kappa\, a^T \mu) \tag{3}$$

with $\kappa \geq 0$, $\|\mu\| = 1$ and C_3 a normalization constant given by

$$C_3(\kappa) = \frac{\kappa}{4\pi \sinh(\kappa)} = \frac{\kappa}{2\pi(e^\kappa - e^{-\kappa})} \quad . \tag{4}$$

Examples of estimated PDFs p_1 and p_2 are shown in Figure 1.

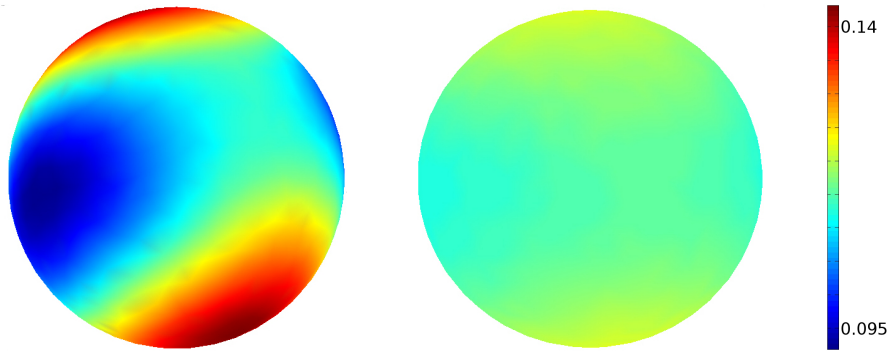

(a) (b)

Fig. 1. Example of estimated probability density functions of the diffusion direction at voxels belonging to the tracked fiber bundle (a) and of the diffusion direction at voxels belonging to the background (b). For visualization purposes, the whole sphere is shown and not only the upper hemisphere to which we restrict our computations. Notice the strong directional preference in voxels belonging to the tracked bundle.

PDF-XChange Viewer Click to buy NOW! www.docu-track.com
PDF-XChange Viewer Click to buy NOW! www.docu-track.com

3.2 Fuzzy Membership Formulation

Once the PDFs p_1 and p_2 have been estimated, we suggest minimizing the following energy functional

$$F(u,p_1,p_2)=\int_\Omega |\nabla u(x)|\,dx+\lambda\int_\Omega \{u(x)\cdot[-p_1(I(x))]+(1-u(x))\cdot[-p_2(I(x))]\}\,dx. \tag{5}$$

The first term of the energy functional is a regularization term that minimizes the total variation of u, i.e. the sum of the perimeters of its level sets, and thus guarantees the smoothness of the segmented region. The second term, weighted by a scalar $\lambda>0$, is the fuzzy competition term which drives the membership function u towards the region of higher probability. In order to minimize F, we follow the approach described in [11] in a related context: we introduce an auxiliary variable v and minimize the approximation to F given by

$$\begin{aligned}\tilde{F}(u,v,p_1,p_2)=&\int_\Omega |\nabla u(x)|\,dx+\frac{1}{2\theta}\int_\Omega |u(x)-v(x)|^2\,dx\\&+\lambda\int_\Omega \{v(x)\cdot[-p_1(I(x))]+(1-v(x))\cdot[-p_2(I(x))]\}\,dx\end{aligned} \tag{6}$$

with respect to the minimizing couple (u^*,v^*). The scalar θ is chosen to be small, so that u^* and v^* are almost identical. The optimal v^* may be computed as [11]

$$v^*(x)=\min(\max(0,u(x)-\theta r(x)),1) \tag{7}$$

where the error function $r(x)$ is given by $r(x)=\lambda\cdot[p_2(I(x))-p_1(I(x))]$. For simplicity and efficiency, having already evaluated the PDFs p_1 and p_2 on n approximately evenly distributed points on $\mathcal{A}$, we evaluate the PDFs at $I(x)$ by using nearest-neighbor interpolation. It is easy to see that Equation (7) updates $v(x)$ to indicate a membership to the most likely region. We are now left with the minimization of the membership function u. In the form of Equation (6), only the first two terms of $\tilde{F}$ depend on u, which are exactly the functional minimized in [12] to obtain an image of minimized total variation u from a noisy image v. Let us review the algorithm suggested in [12] to solve the total variation minimization problem and extend it to the three dimensional case. For an image q of size $N_x\times N_y\times N_z$ the gradient ∇q at (i,j,k) is defined as the vector (q_x,q_y,q_z). For example, the partial derivative in x-direction is approximated by

$$q_x(i,j,k)=\begin{cases}q(i+1,j,k)-q(i,j,k) & \text{if } i<N_x\\ 0 & \text{if } i=N_x\end{cases} \tag{8}$$

PDF-XChange Viewer Click to buy NOW! www.docu-track.com
PDF-XChange Viewer Click to buy NOW! www.docu-track.com

and respectively in the other dimensions. For a vector-valued image p of size $N_x \times N_y \times N_z \times 3$, the divergence operator div p is defined as

$$
\begin{aligned}
(\text{div } p)(i,j,k) = &\begin{cases} p(i,j,k,1) - p(i-1,j,k,1) & \text{if } 1 < i < N_x \\ p(i,j,k,1) & \text{if } i = 1 \\ -p(i-1,j,k,1) & \text{if } i = N_x \end{cases} \\
+ &\\
&\begin{cases} p(i,j,k,2) - p(i,j-1,k,2) & \text{if } 1 < j < N_y \\ p(i,j,k,2) & \text{if } j = 1 \\ -p(i,j-1,k,2) & \text{if } j = N_y \end{cases} \\
+ &\\
&\begin{cases} p(i,j,k,3) - p(i,j,k-1,3) & \text{if } 1 < k < N_z \\ p(i,j,k,3) & \text{if } k = 1 \\ -p(i,j,k-1,3) & \text{if } k = N_z \end{cases}
\end{aligned} \tag{9}
$$

In three dimensions, it can be shown (the proof is similar to the 2D case in [12]) that for $\tau \leq 1/12$, $p^0 = 0$ and

$$
p^{n+1}(i,j,k,\cdot) = \frac{p^n(i,j,k,\cdot) + \tau(\nabla(\text{div } p^n - v/\theta))(i,j,k,\cdot)}{1 + \tau|(\nabla(\text{div } p^n - v/\theta))(i,j,k,\cdot)|} \tag{10}
$$

the series

$$
v - \theta \text{div } p^{n+1} \tag{11}
$$

converges to the optimal solution u^* as $n \to \infty$. Similarly to the remark in the original paper that setting $\tau = 1/4$ still seems to lead to convergence for the 2D case, from our experience in 3D the algorithm appears to work well for $\tau = 1/6$ as well.

3.3 Overview of the algorithm

Summarizing, for a given tolerance $t_s \geq 0$, our algorithm works as follows:

- obtain initial guess for the segmentation of the fiber tract by means of a fiber tracking algorithm
- initialize u^0 to 1 at voxels pierced by the tracked fibers and to 0 elsewhere
- while $|u^{n+1} - u^n|_\infty > t_s$
  - estimate the PDFs p_1 and p_2 according to Equations (1) and (2)
  - set $v := u$
  - update v according to Equation (7)
  - minimize the total variation of u according to Equation (11)
- threshold u to obtain the segmented fiber tract

PDF-XChange Viewer Click to buy NOW! www.docu-track.com
PDF-XChange Viewer Click to buy NOW! www.docu-track.com

3.4 Local Adaptation

In order to estimate the PDFs of the principal diffusion direction not globally on the whole image but locally, we suggest applying the algorithm multiple times on subimages centered at the centerline of the tracked fibers, as schematically illustrated for a synthetic image in Figure 2(a). In our implementation we compute the centerline by simply averaging the coordinates of the tracked fibers, although more complicated skeletonization approaches such as the ones described in [14,15] may be used. Another simple option is to split the image into multiple images along one dimension, and subsequently compute a box around the tracked fibers in the remaining two dimensions.

4 Results

We test our algorithm on two synthetic datasets with varying amount of image noise and on one real image. As suggested in [16], Rician distributed noise may be simulated in a magnitude MR image by computing $|E(\mathbf{q}, \Delta) + \tilde{N}(0, \sigma^2)|$, where $E(\mathbf{q}, \Delta)$ is the attenuated MR signal and $\tilde{N}(0, \sigma^2)$ is a Gaussian distributed complex variable with mean 0 and variance σ^2.

For both synthetic datasets, we use the parameters $\kappa = 1$, $\theta = 10$, $\lambda = 1$, $t_s = 0.1$, $t_{TV} = 0.01$. t_{TV} is the threshold parameter on the maximal difference between u^{n+1} and u^n when iteratively minimizing the total variation of u. For the real dataset we choose $\lambda = 0.5$, preferring a slightly lower competition factor because of potentially similar directions in foreground and background.

The first dataset is given by a torus-shaped DTI phantom. For details on the construction of the model, see [7]. The model presents a fiber bundle shaped as part of a torus, surrounded by highly isotropic tensors with random principal diffusion direction. The b_0 image is shown in Figure 2(a), together with the labeling of the seed ROI used for fiber tracking and the subimages along the centerline of the bundle to which our algorithm is applied. An example noisy b_0 subimage ($\sigma = 6$) is shown in Figure 2(b), and results of the variational segmentation algorithm are displayed in Figure 2(e) and 2(f). The generated segmentation results are compared to the original mask obtained by means of fiber tracking and to the min-cut based approach presented in [10], by computing the corresponding Dice's similarity coefficient [35]. Results for the torus-shaped phantom are presented in Table 1.

Noise Standard Deviation	**2.0**	**4.0**	**6.0**
original mask after fiber tracking	0.844	0.771	0.654
after applying the variational segmentation algorithm	**0.957**	**0.945**	**0.939**
after applying the min-cut based segmentation algorithm	0.923	0.918	0.918

Table 1. Comparison of Dice's coefficients for the torus-shaped model.

PDF-XChange Viewer Click to buy NOW! www.docu-track.com
PDF-XChange Viewer Click to buy NOW! www.docu-track.com

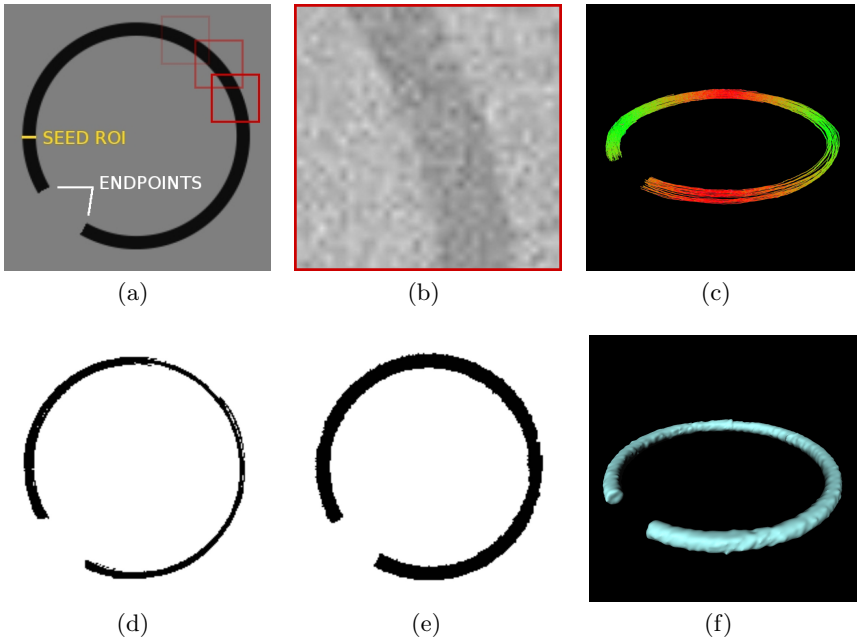

Fig. 2. (a) The b_0 image of the torus-shaped DTI phantom with labeled seed ROI used for fiber tracking and the subimages along the centerline of the bundle to which our algorithm is applied (delineated by the red boxes). (b) Example noisy b_0 subimage ($\sigma = 6$). (c) Result of fiber tracking. (d) One slice of the mask used to initialize the segmentation algorithm, given by the voxels pierced by the tracked fibers. (e) Resulting mask after applying the variational segmentation algorithm and thresholding. (f) Segmentation result displayed in 3D as iso-surface.

Next, we test our algorithm on a DTI phantom based on the BrainWeb project [13], with which we realistically modeled part of the right corticospinal tract (details on the model can be found in [6]). Both the tensors which are part of the tract and the tensors in the background have approximately the same anisotropy. Examples of tracked fibers are shown in Figure 3(a), and an example color coding of the membership function u is presented in Figure 3(b). Segmentation results for different noise levels are given in Table 2.

Noise Standard Deviation	**2.0**	**4.0**	**6.0**
original mask after fiber tracking	0.702	0.610	0.640
after applying the segmentation algorithm	**0.888**	**0.868**	**0.862**
after applying the min-cut based segmentation algorithm	0.849	0.831	0.768

Table 2. Comparison of Dice's coefficients for the BrainWeb-based model.

PDF-XChange Viewer Click to buy NOW! www.docu-track.com
PDF-XChange Viewer Click to buy NOW! www.docu-track.com

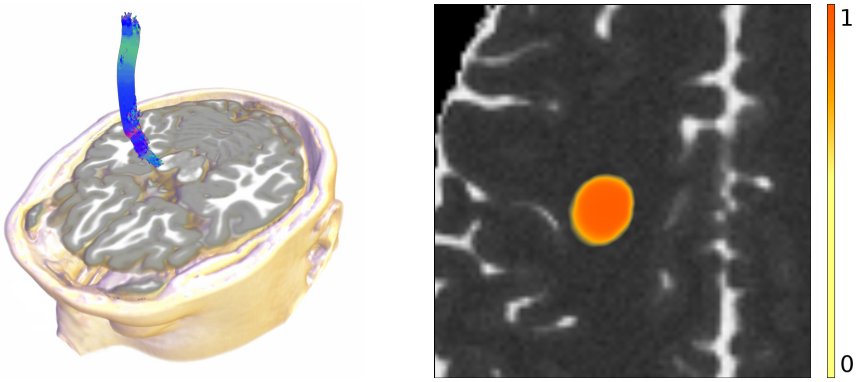

(a) (b)

Fig. 3. (a) Example of fibers tracked on the BrainWeb-based DTI phantom, in which we modeled part of the corticospinal tract. (b) The fuzzy membership function u is color coded and overlaid on a slice of the modeled b_0 image (noise σ=6).

Finally, we test our algorithm on a real magnetic resonance dataset of a tumor patient (diffusion-weighted images with TR/TE/FA = 10700ms/84ms/90°, voxel size is 1.80×1.80×1.98mm, source: [17]) on which we track the corticospinal tract. We assume that the surgeon performing fiber tracking considers the tracked fibers to be part of the bundle he would like to segment, therefore for this dataset we do not allow for voxels to be excluded from the initial segmentation mask, but only included. The resulting segmentation is visualized in 2D by color coding the membership function u (see Figure 4(a)) and in 3D as a semi-transparent hull around the tracked fibers (see Figure 4(b)). A non-optimized Matlab [24] implementation of the algorithm on a modern PC (Intel Core2 Quad CPU) took approximately 30 minutes to segment the image.

5 Discussion

With this work, we have presented a novel variational approach to the segmentation of DTI data. The algorithm consists of two steps which are alternated in an iterative fashion: the estimation of the PDFs of the principal diffusion directions in the tract to be segmented and in the image background, followed by the minimization of an energy functional which drives voxels to the most likely region based on the principal diffusion direction in that voxel, and guarantees a smooth partition of the image by minimizing the total variation of the membership function u.

Our first tests on both synthetic data (which we could quantitatively analyze by comparing Dice's similarity coefficients) and a real dataset support the validity of the method. The Dice's coefficients are a bit lower for the BrainWeb-based phantom, which may be due to excessive smoothness imposed on the segmenta-

PDF-XChange Viewer Click to buy NOW! www.docu-track.com
PDF-XChange Viewer Click to buy NOW! www.docu-track.com

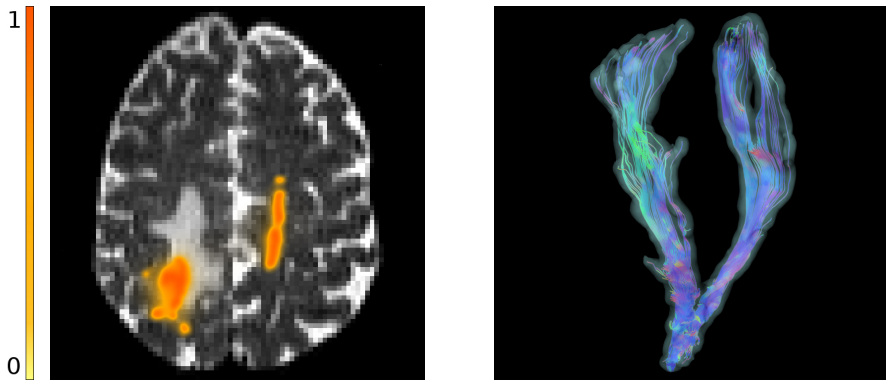

(a) (b)

Fig. 4. The corticospinal tract of a tumor patient has been tracked and successively segmented. In (a) the fuzzy membership function u is color coded and overlaid on a slice of the original b_0 image. In (b) the segmentation result after thresholding is visualized as a semi-transparent hull around the tracked fibers.

tion result in regions near the cortex where the phantom presents an irregular border. An optimization of the parameters will be considered in future work, in addition to an in-depth analysis of the stability of the computed fuzzy membership function with respect to different initializations (i.e., different parameters used for the initial fiber tracking) and modeling of the underlying tensor data. Moreover, extensive analysis is needed in order to determine an appropriate threshold value for the likelihood function, depending on the properties (such as image noise and resolution) of the considered dataset.

Two positive indications may be inferred from the segmentation results on the synthetic test data. As a first remark, being based on an analysis of the principal diffusion directions of the tensors, the algorithm seems to perform well both when there is a large anisotropy difference between the two regions (torus-shaped model) and when the difference mainly lies in the principal diffusion direction (BrainWeb-based model). As a second remark, the algorithm seems to produce segmentation results of comparable quality when different levels of image noise are modeled. Finally, higher segmentation accuracy was obtained compared to the graph-based approach from [10].

An interesting idea for future work may be to estimate the variance-covariance matrix of the principal diffusion direction in each voxel according to the framework presented in [19,20,21] and make use of the obtained data for a pointwise kernel density estimation of the PDFs of the principal diffusion directions. This way, particularly noisy voxels could contribute less to the estimated PDFs. The algorithm should also be extended to make use of information on fractional anisotropy, or on all six tensor entries, to better deal with the case of crossing or kissing fibers.

PDF-XChange Viewer Click to buy NOW! www.docu-track.com
PDF-XChange Viewer Click to buy NOW! www.docu-track.com

In conclusion, we hope that after an accurate analysis of the stability of the suggested method, the algorithm may be helpful for presurgical planning and various clinical studies.

Acknowledgments

This project was funded in part by the German Research Society (DFG PE199/21-1 & DFG NI568/3-1).

References

1. Arsigny, V., Fillard, P., Pennec, X., Ayache, N.: Log-euclidean metrics for fast and simple calculus on diffusion tensors. Magn. Reson. Med. 56, 411–421 (2006)
2. Awate, S., H., Gee, J.: Dispersion on a sphere. In: Proc. Roy. Soc. London Ser. A. vol. 217, pp. 295–305 (1953)
3. Awate, S., H., Gee, J.: A fuzzy, nonparametric segmentation framework for dti and mri analysis. In: Proc. Inf. Process Med. Imaging. pp. 296–307 (2007)
4. Awate, S., Zhang, H., Gee, J.: Fuzzy Nonparametric DTI Segmentation for Robust Cingulum-Tract Extraction. Lect. Notes Comput. Sci., Springer, Berlin, Germany (2007)
5. Awate, S., Zhang, H., Gee, J.: A fuzzy, nonparametric segmentation framework for dti and mri analysis: With applications to dti-tract extraction. IEEE Trans. Med. Imaging 26, 1525–1536 (2007)
6. Barbieri, S., Klein, J., Nimsky, Ch., Hahn, H.: Assessing fiber tracking accuracy via diffusion tensor software models. In: Proc. SPIE Medical Imaging (2010)
7. Barbieri, S., Klein, J., Nimsky, Ch., Hahn, H.: Towards image-dependent safety hulls for fiber tracking. In: Proc. ISMRM (2010)
8. Basser, P.: Fiber-tractography via diffusion tensor MRI (DT-MRI). In: Proc. Int. Soc. Magn. Reson. Med. (1998)
9. Basser, P., Mattiello, J., LeBihan, D.: MR diffusion tensor spectroscopy and imaging. Biophys. J. 66(1), 259–267 (1994)
10. Bauer, M., Egger, J., O'Donnell, T., Barbieri, S., Klein, J., Freisleben, B., Hahn, H., Nimsky, Ch.: A fast and robust graph-based approach for boundary estimation of fiber bundles relying on fractional anisotropy maps. In: Proc ICPR (2010)
11. Bresson, X., Esedoglu, S., Vandergheynst, P., Thiran, J.P., Osher, S.: Fast global minimization of the active contour/snake model. J. Math. Imaging Vis. 28, 151–167 (2007)
12. Chambolle, A.: An algorithm for total variation minimization and applications. J. Math. Imaging Vis. 20, 89–97 (2004)
13. Collins, A., Zijdenbos, A., Kollokian, V., Sled, J., Kabani, N., Holmes, C., Evans, A.: Design and construction of a realistic digital brain phantom. IEEE Trans. Med. Imaging 17(3), 463–468 (1998)
14. Cornea, N., Silver, D., Min, P.: Curve-skeleton properties, applications, and algorithms. IEEE Trans. Vis. Comput. Graph. 13, 530–548 (2007)
15. Cornea, N., Silver, D., Yuan, X., Balasubramanian, R.: Computing hierarchical curve-skeletons of 3d objects. Visual. Comput. 21, 945–955 (2005)
16. Hahn, H., Klein, J., Nimsky, Ch., Rexilius, J., Peitgen, H.O.: Uncertainty in diffusion tensor based fiber tracking. Acta Neurochir. Suppl. 98, 33–41 (2006)

PDF-XChange Viewer Click to buy NOW! www.docu-track.com
PDF-XChange Viewer Click to buy NOW! www.docu-track.com

17. IEEE Vis. Contest. Image Data, Case 1: http://viscontest.sdsc.edu/2010/ (2010)
18. Jonasson, L., Bresson, X., Hagmann, P., Thiran, J., Wedeen, V.: Representing diffusion mri in 5-d simplifies regularization and segmentation of white matter tracts. IEEE Trans. Med. Imaging 26(11), 1547–1554 (2007)
19. Koay, C., Chang, L.C., Carew, J., Pierpaoli, C., Basser, P.: A unifying theoretical and algorithmic framework for least squares methods of estimation in diffusion tensor imaging. J. Magn. Reson. 182, 115–125 (2006)
20. Koay, C., Chang, L.C., Pierpaoli, C., Basser, P.: Error propagation framework for diffusion tensor imaging via diffusion tensor representations. IEEE Trans. Med. Imaging 26(8), 1017–1034 (2007)
21. Koay, C., Nevo, U., Chang, L.C., Pierpaoli, C., Basser, P.: The elliptical cone of uncertainty and its normalized measures in diffusion tensor imaging. IEEE Trans. Med. Imaging 27(6), 834–846 (2008)
22. Lenglet, C., Rousson, M., Deriche, R.: Dti segmentation by statistical surface evolution. IEEE Trans. Med. Imaging 25(6), 685–700 (2006)
23. Mardia, K., Jupp, P.: Directional Statistics. Wiley Series in Probability and Statistics, Wiley, Chichester, U.K. (1999)
24. Matlab: The MathWorks, Inc., Natick, MA
25. Mori, S., Crain, B., Chacko, V., Van Zijl, P.: Three-dimensional tracking of axonal projections in the brain by magnetic resonance imaging. Ann. Neurol. 45(2), 265–269 (1999)
26. Mory, B., Ardon, R.: Fuzzy region competition: A convex two-phase segmentation framework. In: Proc. SSVM. pp. 214–226 (2007)
27. Mory, B., Ardon, R., Thiran, J.P.: Variational segmentation using fuzzy region competition and local non-parametric probability density functions. In: Proc. ICCV. pp. 1–8 (2007)
28. Neil, J., Shiran, S., McKinstry, R., Schefft, G., Snyder, A., Almli, C., Akbudak, E., Aronovitz, J., Miller, J., Lee, B., Conturo, T.: Normal brain in human newborns: apparent diffusion coefficient and diffusion anisotropy measured by using diffusion tensor MR imaging. Radiology 209, 57–66 (1998)
29. Parker, G., Wheeler-Kingshott, C., Barker, G.: Estimating distributed anatomical connectivity using fast marching methods and diffusion tensor imaging. IEEE Trans. Med. Imaging 21(5), 505–512 (2002)
30. Parzen, E.: On estimation of a probability density function and mode. Ann. Math. Statist. 33, 1065–1076 (1962)
31. Pierpaoli, C., Basser, P.: Toward a quantitative assessment of diffusion anisotropy. Magn. Reson. Med. 36, 893–906 (1996)
32. Schlüter, M., Konrad-Verse, O., Hahn, H., Stieltjes, B., Rexilius, J., Peitgen, H.O.: White matter lesion phantom for diffusion tensor data and its application to the assessment of fiber tracking. In: Proc. SPIE Med. Imaging. vol. 5746, pp. 835–844 (2005)
33. Wiegell, M., Tuch, D., Larson, H., Wedeen, V.: Automatic segmentation of thalamic nuclei from diffusion tensor magnetic resonance imaging. Neuroimage 19, 391–402 (2003)
34. Ziyan, U., Tuch, D., Westin, C.F.: Segmentation of thalamic nuclei from DTI using spectral clustering. In: Proc. MICCAI. pp. 807–814 (2006)
35. Zou, K., Warfield, S., Bharatha, A., Tempany, C., Kaus, M., Haker, S., Wells III, W., Jolesz, F., Kikinis, R.: Statistical validation of image segmentation quality based on a spatial overlap index. Acad Radiol. 11(2), 178–189 (2004)